Computers and Concrete, *Vol. 19, No. 5 (2017) 527-535*
DOI: https://doi.org/10.12989/cac.2017.19.5.527

An approach of evaluation and mechanism study on the high and steep rock slope in water conservancy project

Meng Yang[1,2,3a], Huaizhi Su[*1,2,3] and Zhiping Wen[4]

[1]*State Key Laboratory of Hydrology-Water Resources and Hydraulic Engineering, Hohai University, 210098, Nanjing, China*
[2]*College of Water Conservancy and Hydropower Engineering, Hohai University, 210098, Nanjing, China*
[3]*National Engineering Research Center of Water Resources Efficient Utilization and Engineering Safety, 210098, Nanjing, China*
[4]*Department of Computer Engineering, Nanjing Institute of Technology, 211167, Nanjing, China*

(Received September 7, 2016, Revised January 20, 2017, Accepted February 6, 2017)

Abstract. In this study, an aging deformation statistical model for a unique high and steep rock slope was proposed, and the aging characteristic of the slope deformation was better reflected. The slope displacement was affected by multiple-environmental factors in multiple scales and displayed the same tendency with a rising water level. The statistical model of the high and steep rock including non-aging factors was set up based on previous analyses and the study of the deformation and residual tendency. The rule and importance of the water level factor as a non-aging unit was analyzed. A partitioned statistical model and mutation model were established for the comprehensive cumulative displacement velocity with the monitoring study under multiple factors and multiple parameters. A spatial model was also developed to reflect and predict the whole and sectional deformation character by combining aging, deformation and space coordinates. A neural network model was built to fit and predict the deformation with a high degree of precision by mastering its feature of complexity and randomness. A three-dimensional finite element model of the slope was applied to approach the structure character using numerical simulations. Further, a three-dimensional finite element model of the slope and dam was developed, and the whole deformation state was analyzed. This study is expected to provide a powerful and systematic method to analyze very high, important and dangerous slopes.

Keywords: high and steep slope; statistic model; spatial model; neural network; finite element model

1. Introduction

Since 1949, China has constructed approximately 85,000 dams, especially for huge hydropower projects, such as Xiao Wan, Jin Ping, La Xiwa, Tian Shengqiao, Xi Luodu, Long Tan and Shuang Jiangkou, which made China the largest hydropower producer of developing nations worldwide. It also has resulted in many high slope problems (Zhou *et al.* 2006, Su *et al.* 2011, Yang *et al.* 2015a, Chowdary *et al.* 2013). Prof. Leopold Muller noted a slope was not solved very well even though it was the easiest question in rock mechanics (Sevim *et al.* 2014, Abdalla *et al.* 2015). A rock slope safety state affects the project itself and the whole environment around it. The study of a high slope has become very popular in the geotechnical engineering field. The inspection data at the original space position of a slope can really reflect the slope behavior in a 1:1 model test, and they are vitally important when evaluating the safety and forecasts of the deformation tendency (Gu *et al.* 2006, Su *et al.* 2012, Yang *et al.* 2015b). In the 1970s, Prof. Jiuyu Cheng first analyzed the monitoring data of dams in China by setting up a statistical model and inversion analyses for deformation parameters to evaluate the engineering service state (Su *et al.* 2014, Cheng *et al.* 2001, Dai *et al.* 2002). Mathematical methods, such as statistical regression, time series, neural network, and grey system, became a popular way to analyze the monitoring data. The finite element method (FEM) of numerical simulation technology was widely used for geotechnical engineering.

This paper mainly focuses on fusing together the multiple-source information of the specific and enormous high and steep rock slope in the hydropower project and analyzing the deformation behavior in for multiple aspects and multiple levels by constructing a whole sequence statistical model of the comprehensive cumulative displacement using the sectional statistical model and mutation model for the velocity of the comprehensive displacement. The spatial model was based on the coordinate value and environmental factors and was used to analyze and forecast the spatial deformation state for every section of the slope. The neural network was a useful method to evaluate and predict the deformation value. The Drucker-Prager (D-P) criterion was used to determine the safety coefficient by the finite element model. The whole deformation law was also analyzed by a generalized three-dimensional finite element model.

2. Arrangement of monitoring points

∗Corresponding author, Professor
E-mail: su_huaizhi@hhu.edu.cn
[a]Ph.D. Student
E-mail: ymym_059@126.cm

Copyright © 2017 Techno-Press, Ltd.

ISSN: 1598-8198 (Print), 1598-818X (Online)

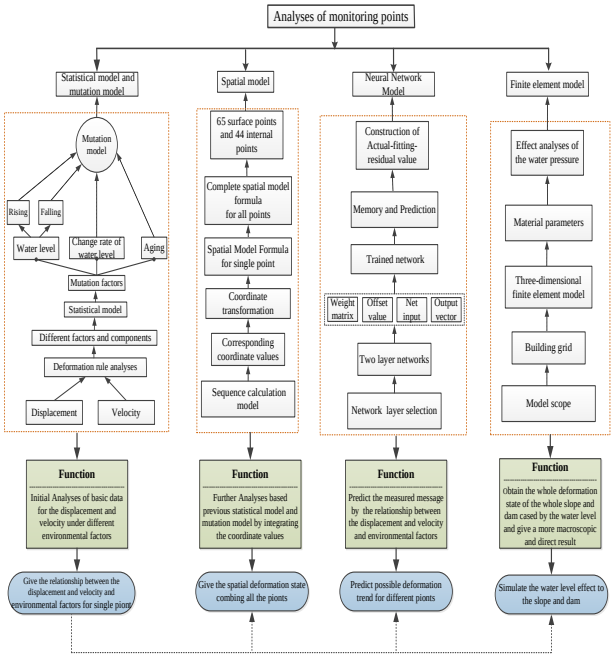

Fig. 1 The function flowcharts for different models

This hydropower project is the second largest step electric station in the Yellow River. It is located at the exit of the Longyang Gorge in the east of the Tibetan Plateau. The slope is at the right of the upstream of the hydropower project. The altitude of the top platform of the slope is 2930 m-2950 m, and it is 750 m long and 50 m-290 m wide with an area of 115, 000 m^2. The quality of monitoring information mainly depends on the arrangement of the monitoring points. The slope includes the top platform, I region, II region and III region, and the main monitoring content is the deformation monitoring, whose points are listed in each section. Approximately 30 various points distributed on the top platform were sampled at an interval of 1-3 days with a measurement accuracy of approximately 1 mm. A plane deformation controlling network and precise leveling network were set as the work basis points at the scarp of the top platform since July, 2009. The deformation monitoring points were arranged at the top platform and continuous data were acquired on the 15th of Aug. 2009. There were approximately 14 artificial points and 12 GPS points at the I region using the polar coordinates method as measured by the total station device. The work basis points were located at an altitude of 2465 m and 2543 m for the left slope, and the frequency was 1-3 days with accuracy of 2 mm-5 mm. The II region was monitored by 20 artificial points and 3 GPS points.

The deformations of different depth levels can be monitored by inside monitoring, including inside horizontal distortion, vertical distortion, tile deformation, underwater level, local crack and dislocation deformation. The horizontal distortion inside was measured by an indium wire horizontal displacement meter, laser range-finder, wide range displacement gage, borehole inclinometer and survey traverse. The inclinometer was installed along and perpendicular to the river using a torsion meter to revise the angle for a consistent installation direction.

Based on previous analyses, the function flowcharts for different models have been presented in Fig. 1.

3. Establishment of the deformation model

The factors influencing the displacement and displacement velocity include water level, aging, rainfall, and temperature, according to the practical monitoring data. The rainfall and temperature has the lowest influence because the region is a low rainfall area. The water level, aging factor and rate of change of the water level are chosen to be the main factors. The deformation statistic model is set up as follows

$$\delta = \delta_H + \delta_\theta + \delta_v \tag{1}$$

where δ is the slope deformation; δ_H is the component of water level; δ_θ denotes the aging factor; and δ_v is the component for change rate of water level.

1. Water level component of δ_H

The water level influences the slope deformation by surface water pressure and seepage water pressure of the reservoir. A hysteresis effect exists with a change in the water level that influences a complex mutual effect between the rock and water. The water level of the early 30 days is chosen, and the water pressure component is expressed as

$$\delta_H = \sum_{i=1}^{3} a_{1i}((h_1 - h_a)^i - (h_0 - h_a)^i) + \sum_{j=2}^{8} a_{2j}((h_j - h_a) - (h_{j0} - h_a)) \tag{2}$$

where h_1 is the current water level; h_a denotes the altitude of the bottom of the reservoir; h_0 is the initial water level; h_j(j=2-8) denotes the average water level of 1 day ago, 2 days ago, 3-4 days ago, 5-7 days ago, 8-11 days ago, 12-16 days ago and 17-30 days ago, respectively; h_{j0} denotes the corresponding initial water level; and a_{1i} and a_{2j} denote the regression coefficients of the water level factor.

2. Aging component of δ_θ

The aging component rule was developed by fitting the measured information. The aging component, which includes the influence of invasion of the reservoir water, the creep of rock and other factors, is as follows

$$\delta_\theta = b_1(\theta - \theta_0) + b_2(\ln(\theta_0 + 0.5) - \ln(\theta + 0.5)) \tag{3}$$

where θ is the cumulative day, t, from the initial day to the monitoring day divided by 500; θ_0 is the cumulative day, t_0, from the initial day to the first measuring day of the model data divide by 500; and b_1 and b_2 are the regression coefficients of the aging factor.

3. Change rate of water level δ_v

The rate of change of the water level is the ratio between the change in value of water level of neighboring days and their interval days. It has a certain influence on the slope deformation for the penetrated water pressure. Taking the change rate and its previous term into consideration, the rate of change component is as follows

$$\delta_v = cv_u + \sum_{k=1}^{3} c_k \left(v_k\right) \tag{4}$$

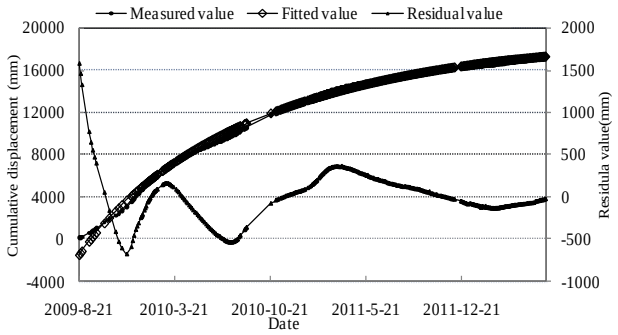

Fig. 2 Measured and fitted data for QC10

where v_u is the water level change rate corresponding to the monitoring day; v_k(k=1-3) is the water level change rate to prior monitoring days, which means the change rate of 1 day ago, 2 days ago and average change rate of 3-4 days ago; and c and c_k are the corresponding regression coefficients.

Based on the previous analyses, the statistic model of the slope displacement is expressed as

$$\delta = b_0 + \sum_{i=1}^{3} a_{1i}((h_1 - h_a)^i - (h_0 - h_a)^i) + \sum_{j=2}^{8} a_{2j}((h_j - h_a) - (h_{j0} - h_a)) + b_1(\theta - \theta_0) + b_2(\ln(0.5+\theta) - \ln(\theta_0 + 0.5)) + cv_u + \sum_{k=1}^{3} c_k(v_k) \quad (5)$$

where b_0 is a constant value.

3.1 Statistical model of the comprehensive accumulation displacement

Deformation is the easiest factor to obtain and is the most obvious. First, the comprehension accumulation displacement is chosen as the effect quantity. Based on the actual condition of the slope, the monitoring point, QC10, with altitude of 2937 m at the top of the platform between the faults of LF53 and LF54, is selected as a typical analysis for its large deformation and long time series. The creep characteristic is the basis for the rock mass deformation. Rheology of the slope was caused by gravity and other external loads, which exhibited creep behavior. Rheology plays a critical factor in the aging deformation. Thus, a statistical model only including the aging factor is as follows

$$\delta = \delta_\theta = b_1(\theta - \theta_0) + b_2(\ln(\theta_0 + 0.5) - \ln(\theta + 0.5)) \quad (6)$$

Based on the multiple correlation coefficient of R of 0.9984 and other combined factors in Fig. 2, some conclusions can be drawn: The model can predict the time rule of deformation, which shows the aging deformation is the main characteristic and matches the basic rock material character for the slope. However, the slope deformation is influenced by not only the aging factor causing aging deformation but also some non-aging factors producing non-aging deformation, such as rainfall, water level, change of water level, etc. The non-aging factors present obvious regularity when analyzing the available data from December, 2009 to February, 2012, which covers the water rising five times. The deformation caused by non-aging factors increases during a period of rising water, while it gradually decreases during a low and stable water level. The value trends toward a smooth value for water rising at a slower velocity and lower rising height. The timetable of the water level is shown in Table 1.

Table 1 Change in the water level

No.	Period	Beginning time (*dd/mm/yyyy*)	End time (*dd/mm/yyyy*)
II	First rising	14/11/2009	18/12/2009
III	Falling	19/12/2009	22/2/2010
IV	Second stable	23/2/2010	10/7/2010
V	Second rising	11/7/2010	10/8/2010
VI	Third stable	11/8/2010	14/1/2011
VII	Third rising	15/1/2011	1/3/2011
VIII	Forth stable	2/3/2011	10/1/2012
IX	Forth rising	11/1/2012	7/3/2012
X	Fifth stable	8/3/2012	13/6/2012
XI	Fifth rising	14/6/2012	2/7/2012

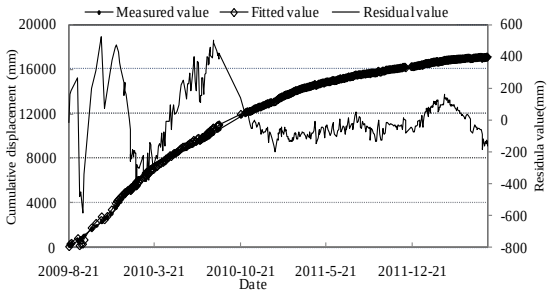

Fig. 3 Measured and fitted data of QC10

It is necessary to consider the factors of water level and its rate, and thus, a slope statistical model is developed

$$\delta = \delta_\theta = b_1(\theta - \theta_0) + b_2(\ln(\theta_0 + 0.5) - \ln(\theta + 0.5)) + \sum_{i=1}^{3}(H_i) + cv_u \quad (7)$$

where H_i denote the first-order, squared and cubic terms for the current water level factor.

The fitted graph is shown in Fig. 3, and the value of R is 0.9995. It is obvious that the water level and its velocity have a large impact on the displacement of the slope besides the aging deformation by comparing the residuals between Figs. 2 and 3.

From the fluctuation rule of the residuals for Fig. 3, some deformation characteristics can be concluded: the residual for a disordered state shows that the main non-aging factors of the slope deformation are water level and its velocity as the water level changes increases, which is caused by the presence of a dam compared to the initial natural condition. The change is the main reason for the non-aging factor. During this process, recoverable and discoverable deformations are generated, and the latter leads to the current large rocky deformation.

3.2 Model of the comprehensive displacement velocity

A single parameter monitoring model can hardly meet

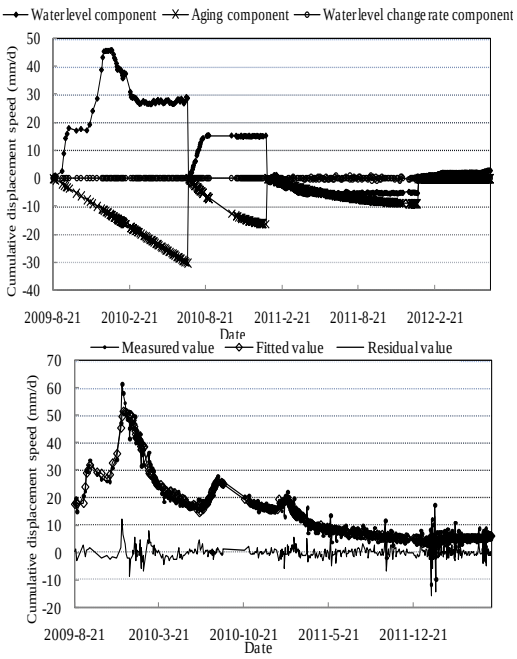

Fig. 4 Graphs of fitting-component-residual for QC10

the modeling demands. Analysis should consider not only the value of the displacement but also the velocity of the deformation. Average daily displacement is chosen as a dependent variable. Simultaneously, the infiltration velocity of the water soaking into the rock is a slow and gradual process that has an impact on the rock. From the analysis of the monitored data, the hysteresis influence for the rock is obvious during this procedure. Based on the previous conclusions, a statistical model of the comprehensive displacement velocity is established to address the mechanics of the water level and principle of rock mechanics, as follows

$$\delta_v = b_0 + \sum_{i=1}^{3} a_{1i}((h_1 - h_a)^i - (h_0 - h_a)^i) + \sum_{j=2}^{8} a_{2j}((h_j - h_a) - (h_{j0} - h_a)) + b_1(\theta - \theta_0) + b_2(\ln(0.5+\theta) - \ln(\theta_0 + 0.5)) + cv_u + \sum_{k=1}^{3} c_k(v_k) \quad (8)$$

There are five periods with a rising water level up to July 2, 2012. The velocity sequence is divided into five stages that consider the differences in the rising periods. The last two periods are combined into one as the amount of monitoring data is smaller than the number of environment factors in the fifth rising period.

The sectionalized statistical model of the comprehension displacement velocity is shown in Eq. (8), and the final result is presented in Fig. 4.

The expressions for the four periods are listed as follows

$$\begin{aligned}
\delta_{v1} &= 6.55+0.94((h_4 - h_a) - (h_{40} - h_a))\text{-}49.28(\theta - \theta_0) \\
\delta_{v2} &= 1.59+0.42((h_3 - h_a) - (h_{30} - h_a))+0.35((h_6 - h_a) - (h_{60} - h_a)) \\
&\quad +246.67(\theta - \theta_0)\text{-}390.62(\ln(0.5+\theta) - \ln(\theta_0 + 0.5)) \\
\delta_{v3} &= 2.42 + 0.42((h_7 - h_a) - (h_{70} - h_a))\text{-}0.94((h_8 - h_a) - (h_{80} - h_a)) \\
&\quad +44.7(\theta - \theta_0)\ \text{-}108.15(\ln(0.5+\theta) - \ln(\theta_0 + 0.5))\text{-}1.75c_3v_3 \\
\delta_{v4} &= 0.18(h_3 - h_a) - (h_{30} - h_a))\text{-}0.98
\end{aligned} \quad (9)$$

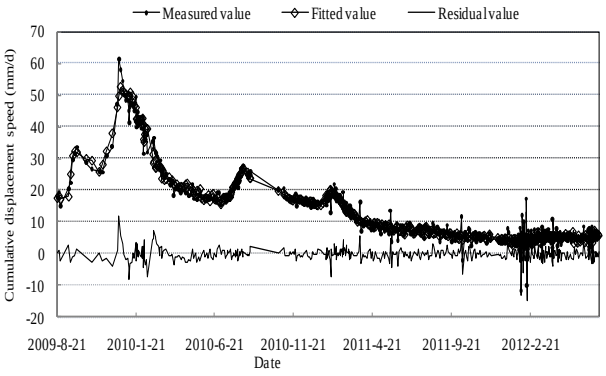

Fig. 5 Graph of fitting-residual for QC10

The velocity is the first derivative of the displacement, reflecting the deformation state between the two observation values, which is another manifestation of the deformation. For this rock slope, the amount of displacement is high and the observation interval is short, which leads to large fluctuations. Based on the previous results of the statistic model and water rising rates of the four segments, 0.75 m/d, 0.22 m/d, 0.18 m/d, 0.44 m/d, the conclusions are as follows: if the water rises quickly, the lag time for water invading the rock decreases. Therefore, rock stabilization is greatly influenced by the fluctuation of the water level. The second graph in Fig. 4 shows the proportion of the aging component, which is one of the dependent variables of the velocity, decreases and gradually approaches zero. It also indicates that the aging of the rock slope trends to be convergent as the change in water level slows down, which means a new stability state appears gradually after prior disturbance.

It is necessary to further analyze the effects of the water level and aging. Therefore, a mutation model is developed, which regards the influence of the aging during five periods as the same rule and considers the effects of the water level, water level change rate and prior water level for rising water in different periods. The model is expressed as follows

$$\begin{aligned}
\delta_v &= b_0 + \sum_{m=1}^{4}\left(\sum_{i=1}^{3} a_{1im}((h_{1m} - h_a)^i - (h_0 - h_a)^i)\right) + \sum_{m=1}^{4}\left(\sum_{j=2}^{8} a_{2jm}((h_{jm} - h_a) - (h_{j0} - h_a))\right) \\
&\quad + b_1(\theta_m - \theta_0) + b_2(\ln(0.5+\theta_m) - \ln(\theta_0 + 0.5)) + \sum_{m=1}^{4}(c_m v_{um}) + \sum_{m=1}^{4}\left(\sum_{k=1}^{3} c_{km}(v_{km})\right)
\end{aligned} \quad (10)$$

In this case, there are in total 58 environmental factors. The specific model expression, with a value of R of 0.9799, is

$$\begin{aligned}
\delta_v &= \text{-}0.234+(3.457H_{11} + 82.474H_{12} - 220.226H_{13} - 0.559H_{22} + 1.518H_{23} + 0.009H_{24} \\
&\quad +0.001H_{32} - 0.003H_{33}) + (-1.014h_{11} - 0.6233h_{13} - 0.747h_{23} + 3.010h_{24} + 1.765h_{31} \\
&\quad -2.715h_{34} - 2.715h_{41} - 0.257h_{51} + 1.038h_{52} + 0.273h_{63} + 0.273h_{63} - 0.5999h_{72} - 0.7147h_{73}) \\
&\quad +(18.631s_1 - 60.023s_2) + (-1.304v_1 - 3.182v_4) + (2.041v_{21} + 1.851v_{23} - 1.943v_{31} - 1.5696v_{33})
\end{aligned} \quad (11)$$

This model has no obvious segmented parts, and the whole sequence is determined; thus, the different effects from rising water are taken into account. The model result is not worse than the segmented model. It can well solve the problem caused by different values of b_0 in each segmented model. It is powerful when comparing the impact state of each environmental unit of rock deformation during different water rising periods. The change of the rock

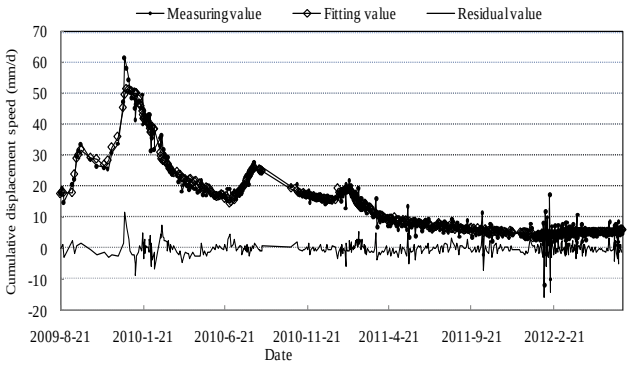

Fig. 6 Graph of the fitting-residual for QC10

deformation with time is not consistent. There are still many other unknown factors besides the water level, such as a seismic wave from far away and rock excavation, which all can be attributed to the aging factor. Therefore, the influence rule of aging in different periods varies greatly.

The mutation model covering aging, water level and velocity of water level is established

$$\delta_v = \sum_{m=1}^{4} b_m + \sum_{m=1}^{4}(\sum_{i=1}^{3} a_{1im}((h_{1m}-h_a)^i-(h_0-h_a)^i)) + \sum_{m=1}^{4}(\sum_{j=2}^{8} a_{2jm}((h_{jm}-h_a)-(h_{j0}-h_a))) + \sum_{m=1}^{4}(b_{1m}(\theta_m-\theta_0)+b_{2m}(\ln(0.5+\theta_m)-\ln(\theta_0+0.5))) + \sum_{m=1}^{4}(c_m v_{um}) + \sum_{m=1}^{4}(\sum_{k=1}^{3} c_{km}(v_{km})) \quad (12)$$

The result of every section for this model is better than the one neglecting the impact rule difference of the aging factor in every period. The value of R is larger than 0.93, except for the fourth section that had a small data set. The problem with a constant influence in every stage will not appear. Each phase has 16 environmental variables that consider all the different rules of all the factors in every stage. The mutation problem of the environmental element in different periods is finally solved well.

4. Establishment of a spatial model

A comprehensive monitoring system that included the slope platform, bank slope, exploration hole and geological drilling monitored the phenomena of deformation since May, 2009. Various monitoring programs were promoted, and complete monitoring information was obtained. Therefore, a spatial model of the rock slope was established by the aspect of spatial dimension so that the multiple-source information can be fully used, and the deformation state can be analyzed from all sides. The model is rational, intuitive, accurate and comprehensive.

First, the spatial model is set up combing the previous whole sequence calculation model with their corresponding coordinate values.

$$\delta_v = e^{\frac{(x-\mu)^2}{2\sigma^2}}(\sum_{i=0}^{3} y^i \sum_{j=0}^{3} \alpha_j z^j)((\theta-\theta_0)+(\ln(0.5+\theta)-\ln(\theta_0+0.5))+\sum_{i=1}^{3}((h_1-h_a)^i-(h_0-h_a)^i)) \quad (13)$$

where X, Y and Z represent the three dimensional coordinates of each measured point.

For the above formula, X and Y replace the north and east direction of the slope, which is different from the world

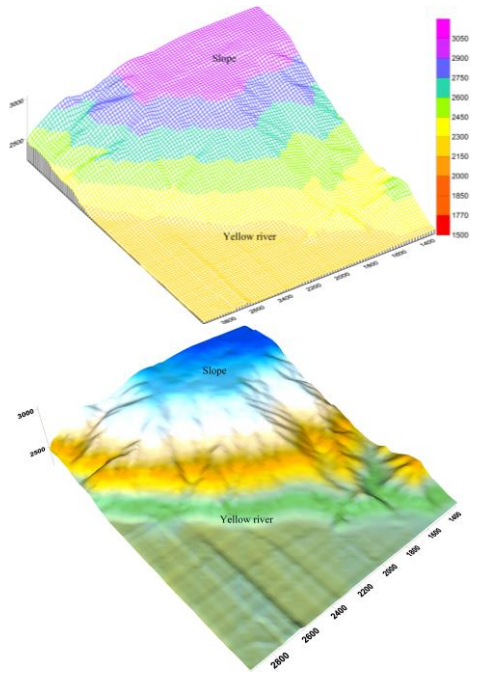

Fig. 7 Interpolated contour map of the slope

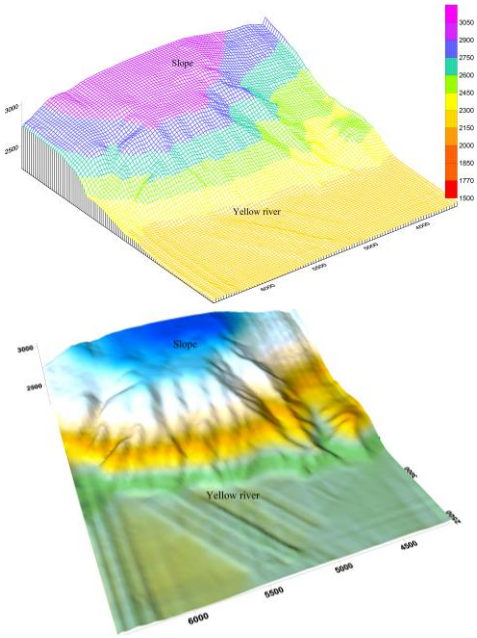

Fig. 8 Interpolated contour rotation map of the slope after revolving

coordinates. The positions of X and Y coordinates should be exchanged when the coordinate data are referred to. The displacement of the slope along the north direction is great in the middle and small at either end. Based on this feature, the normal distribution is used along the X direction and a sixth-ordered polynomial of all factors is adopted in the Y and Z directions, for which no specific rule is used. The water level and aging influences are also considered. The spatial model is finally established. Based on the monitoring condition of the measured point, the points for a short series and small deformation are rejected; thus, 65 surface points and 44 internal points remained.

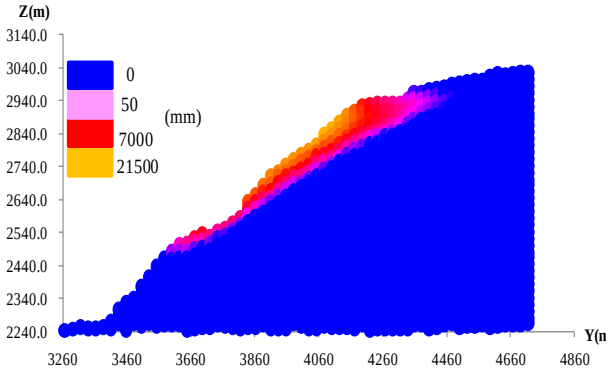

Fig. 9 The cross section of the displacement distribution for QC10 calculated using the spatial model

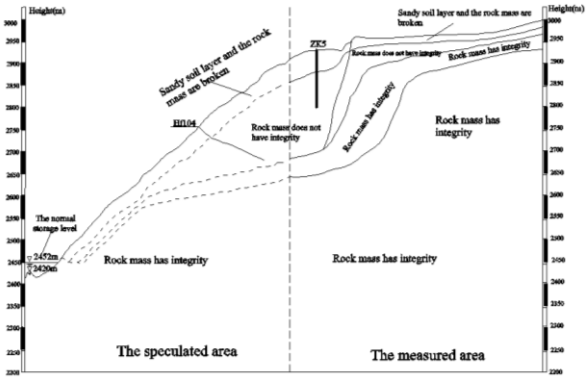

Fig. 10 Deduction figure of the geoelectric cross section of III#

As shown in Fig. 7, this slope takes on a convex status curved to the river bed as a whole, roughly towards NE30°, with the upstream part deflecting slightly to the N-direction. The slope is at an incline of 43 degrees. To ensure its deformation law is the true north and east, a coordinate transformation formula is used

$$\begin{pmatrix} s \\ t \end{pmatrix} = \begin{pmatrix} \cos\beta & -\cos\beta \\ \sin\beta & \sin\beta \end{pmatrix} \begin{pmatrix} x \\ y \end{pmatrix} \tag{14}$$

The grid drawing produced by the coordinate using Eq. (14) is shown in Fig. 8.

According to the previous basic process and Eq. (13), the spatial model calculation containing 109 measured points was developed using a program based on a MATLAB tool. The coefficient of each factor can be calculated. *X*, *Y* and *Z* direction data of the contour point can be extracted from the contour information. The Kriging interpolation algorithm is adapted for the *Y* and *Z* directions of the measured points after conversion, with an interval of 20 m. Then, the interpolation table of measured points on the slope surface can be generated. A cross section passing the QC10 point, vertical to the true north, is established and shown in Fig. 9.

Some new points are produced by the interpolation method based on the coordinate of monitored points and the displacement value of the new interpolating point using Eq. (14). Then, the distribution nephogram is drawn to describe the deformation state of the whole cross section clearly.

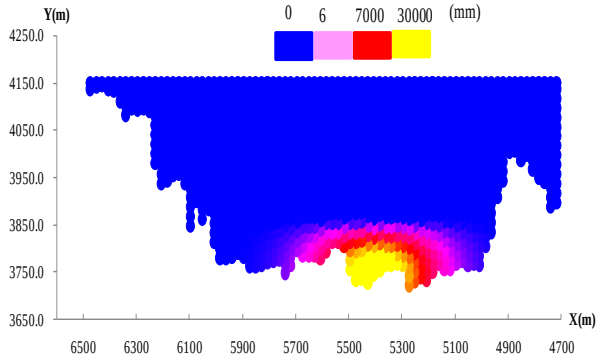

Fig. 11 Cross-sectional nephogram of the displacement for the 2600 m elevation

The EH4 double source magneto-telluric sounding system was used to detect and analyze the typical deep surface. Four cross-monitored lines of I#, II#, III# and VI# are arranged. The deep rock structure characteristic of III# was determined, as show in Fig. 10.

The fitting result of Fig. 9 is basically consistent with the detection result of Fig. 10. The surface rock is broken and has a large deformation; the inside rock will be harder with a small displacement. These conclusions verified that the loose rocks of the surface and unstable structure of superficial active parts contacting with the surface are the main regions easily affected by external environment factors. These analyses also provide a powerful explanation for the deformation of the slope.

The accuracy of the spatial model has been verified, and its application for analyzing the displacement status along the height-direction is performed. The method is the same as the previous one used, and the result is shown in Fig. 11.

The calculation result, corresponding to Fig. 11, shows that the deformation is small when close to the inside rock and that the displacement value is large at a short distance from the river. The largest cumulative displacement is located at the outer edge of the river; the rocks of this region are broken and contact the external environment directly. They are easily affected by all factors. The steady state might be destroyed at the beginning during the construction of dam by construction blasting, excavation, water level rising, and heavy rainfall, among others. The most notable performance occurs in the outer surface of the broken rock, which matches the basic rock mechanics laws and practical monitoring results.

Based on previous analyses for different scales and dimensions, the deformation law and magnitude of the rock are predicted and mastered. The result is consistent with the actual monitoring situation. It is more intuitive to analyze the basic deformation situation for a slope surface. This method provides a new reliable approach to evaluate, analyze and predict the rock slope. The easy realization makes it a practical application to use during construction, operation and management for these high and steep rock slopes. It is also meaningful for analyzing and judging the monitoring data.

5. Analysis of a neural network model

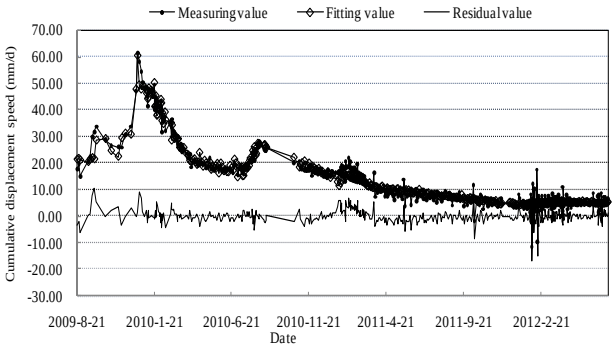

Fig. 12 Actual-fitting-residual value of the velocity of the accumulative displacement for QC10

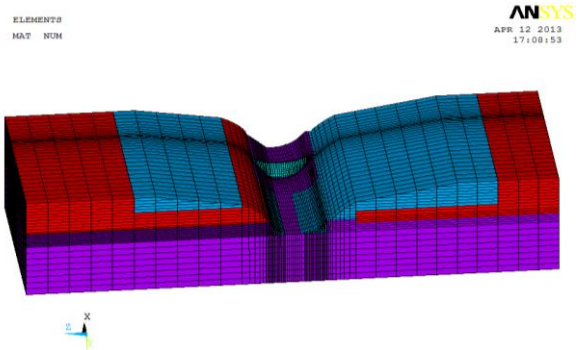

Fig. 13 Generalized three-dimensional finite element model of the slope and arch dam

The neural network has only 2-3 layers included. Each layer has its own weight matrix, offset value vector, net input vector and output vector. Two layer networks are used for the slope monitoring data, which is easier to generalize and has high prediction accuracy. First, the trained network is operated for the velocity of the comprehensive displacement, which means the network of QC10 has the ability of associative memory and prediction. The graph of the actual-fitting-residual is shown in Fig. 12.

The neural network model is a powerful approach to predict the measured message of the high slope because an analysis of the influencing factor of the measuring data is unnecessary according to the fitting results. The beginning models are the best choice to divide and extract the separate hidden factors in the measured source since very high predictive ability is unnecessary.

6. Determination of the safety factor for the slope

A slope is inevitable during construction of water conservancy engineering projects. The stability of the slope seriously affects the safety of construction and operation. How the sliding swell of the dam affected electrical equipment and accumulated landslides close to the dam were serious concerns; it is necessary to analyze the slope stability. The deformation forms of the slope mainly contain relaxation tensile fracture, slide, collapse, dumping, peristalsis, and flow, among others. The mechanical property parameters, geometric dimensions and external loads are the main factors that influence the slope stability

Table 2 Material parameters

Structure type	Compression strength (MPa)	Deformation modulus (GPa)	Rock shear parameters		Poisson's ratio	Unit weight (g/cm^3)
			φ_1	C'(MPa)		
Exterior margin	42	0.77	22.53	0.1857	0.36	2.49
Trailing edge	74	1.35	24.98	0.029	0.32	2.62
Basis	12	2.05	28.96	0.072	0.23	2.69
Dam body	/	22 (elastic modulus)	/	/	0.16	2.43

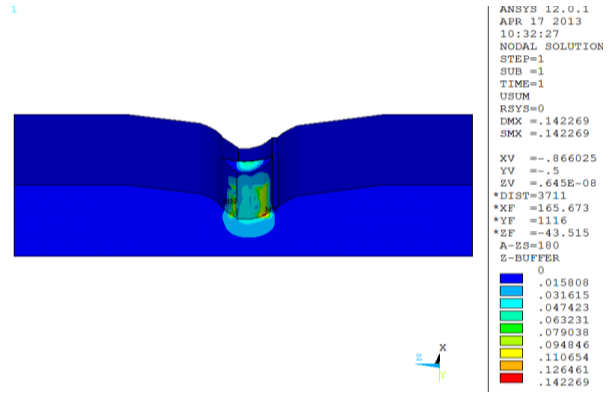

Fig. 14 Nephogram of the equivalent stress

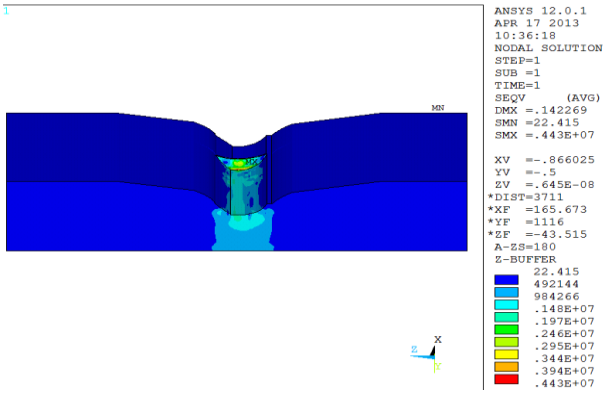

Fig. 15 Nephogram of the equivalent displacement

(Abdul-Rahman *et al.* 2013, Altunisik *et al.* 2015, Bahsan *et al.* 2014, Dejus *et al.* 2013, Finozzi *et al.* 2015).

There are two common methods for analyzing the slope stability: the limit equilibrium method and numerical analysis method. The first method is to divide a landslide into several vertical strips to calculate the safety coefficient by balancing the equation of forces established by the Mohr-Coulomb shear strength theory. The second method overcomes the shortcoming of the former method, which is neglecting the stress-strain relationship of the soil. The FEM is the earliest and the most widely used numerical analysis method (Mazars *et al.* 2015, Bozzano *et al.* 2010, Mehdi *et al.* 2011).

A general three-dimensional finite element model of the slope and dam was set up, and the influence of the water level was further investigated. The model is shown in Fig. 13. Material parameters are listed in Table 2.

Four main areas are considered. The effect of the water pressure acting on the slope and dam are considered separately. The calculation results are shown in Figs. 14 and

15. The height of the slope is very high, and the water level is only 188 m. The straight impact on the slope is small, which matches the influence of the actual water level component divided from the comprehensive displacement. Therefore, an indirect water level factor, the seepage water pressure, should be the main factor influencing the rock slope along with the geological structure and other factors when compared with the other influencing factors to actual monitoring results.

7. Conclusions

A comprehensive system of the slope engineering including analysis, calculation, explanation and conclusion, was developed in this study. The aging deformation statistical model of this slope reflects well its aging character. However, the deformation of a slope is a combined result of multiple-factor influences in multiple scales. The statistical model consisting of a non-aging factor was established based on the important effect of the water rising. To explore the influence rule further, the sectionalized statistical model and mutation model of the comprehensive displacement velocity were determined. The analysis results match the actual situation and are reasonable. Based on the aspect of the spatial dimension, the spatial model of this rock slope was established considering the spatial coordinate values of the measured points. The deformation distribution of a typical cross-section was calculated and built, which was supported by the practical detection results. Another section along the height-direction was also analyzed by the spatial model. The whole space deformation of the slope was also predicted, which was consistent with the practical measurement. Thereby, a rational, intuitive, accurate and comprehensive spatial model is proven to be a step forward. The neural network model is certified to be a powerful approach to predict the measured message of the high and steep slope based on the complexity and multiple-factor characteristic of the slope.

Numerical analysis method was also used for the slope, and a three-dimensional finite element model of the slope was built. To be consistent with previous analysis, a general three-dimensional finite element model covering the slope and dam was developed. The influence of the water level was separately analyzed using single water pressure acting on the slope and dam. The straight impact on the slope is small, which matches the result of the actual water level component of the comprehensive displacement. An indirect water level factor, seepage water pressure, is speculated to be the main factor.

Acknowledgments

This research has been partially supported by National Natural Science Foundation of China (SN: 51579083, 51479054, 41323001, 51139001), the National Key Research and Development Program of China (SN: 2016YFC0401601), Jiangsu Natural Science Foundation (SN: BK2012036), the Doctoral Program of Higher Education of China (SN: 20130094110010), Open Foundation of State Key Laboratory of Hydrology-Water Resources and Hydraulic Engineering (SN: 20145027612, 20165042112), the Fundamental Research Funds for the Central Universities (Grant No. 2015B25414, 2016B04114).

References

Abdalla, J.A., Attom, M.F. and Hawileh, R. (2015), "Prediction of minimum factor of safety against slope failure in clayey soils using artificial neural network", *Environ. Earth Sci.*, **73**(9), 5463-5477.

Abdul-Rahman, H., Wang, C. and Lee, Y.L. (2013), "Design and pilot run of fuzzy synthetic model (FSM) for risk evaluation civil engineering", *J. Civil Eng. Manage.*, **19**(2), 217-238.

Altunisik, A.C. and Sesli, H. (2015), "Dynamic response of concrete gravity dams using different water modelling approaches: Westergaard, lagrange and euler", *Comput. Concrete*, **16**(3), 429-448.

Bahsan, E., Liao, H.J. and Ching, J. (2014), "Statistics for the calculated safety factors of undrained failure slopes", *Eng. Geol.*, **172**, 85-94.

Bozzano, F., Mazzanti, P., Prestininzi, A. and Mugnozza, G.S. (2010), "Research and development of advanced technologies for landslide hazard analysis in Italy", *Landsl.*, **7**(3), 381-385.

Cheng, K. (2001), "Application of matter element analysis theory for blasting classification of rock", *J. Wuhan Univ. Technol.*, **16**(2), 51-53.

Chowdary, V.M., Chakraborthy, D. and Jeyaram, A. (2013), "Multi-criteria decision making approach for watershed prioritization using analytic hierarchy process technique and GIS", *Wat. Res. Manage.*, **27**(10), 3555-3571.

Dai, F.C. and Lee, C.F. (2002), "Landslide characteristics and slope instability modeling using GIS, Lantau Island. Hong Kong", *Geomorphol.*, **42**(3-4), 213-228.

Dejus, T. and Antucheviciene, J. (2013), "Assessment of health and safety solutions at a construction site", *J. Civil Eng. Manage.*, **19**(5), 728-737.

Finozzi, I.B.N., Berto, L. and Saetta, A. (2015), "Structural response of corroded RC beams: A comprehensive damage approach", *Comput. Concrete*, **15**(3), 411-436.

Gu, C.S. and Wu, Z.R. (2006), "Safety monitoring of dams and dam foundations-theory, methods and their application", *Press Hohai Univ.*, 182-187.

Mazars, J. and Grange, S. (2015), "Modeling of reinforced concrete structural members for engineering purposes", *Comput. Concrete*, **16**(5), 683-701.

Mehdi, K. and Mehdi, B. (2011), "A novel hybridization of artificial neural networks and ARIMA models for time series forecasting", *Appl. Soft Comput.*, **11**(2), 2664-2675.

Sevim, B., Altunisik, A.C. and Bayraktar, A. (2014), "Construction stages analyses using time dependent material properties of concrete arch dams", *Comput. Concrete*, **14**(5), 599-612.

Su, H.Z., Hu, J. Li, J.Y. and Wu, Z.R. (2012), "Deep stability evaluation of high-gravity dam under combining action of powerhouse and dam", *J. Geomech.*, **13**(3), 257-272.

Su, H.Z., Li, J.Y., Cao, J.P. and Wen, Z. (2014), "Macro-comprehensive evaluation method of high rock slope stability in hydropower projects", *Stoch. Environ. Res. Risk Assess.*, **28**(2), 213-224.

Su, H.Z., Wen, Z.P. and Wu, Z.R. (2011), "Study on an intelligent inference engine in early-warning system of dam health", *Wat. Res. Manage.*, **25**(6), 1545-1563.

Yang, M. and Liu, S. (2015a), "Field tests and finite element modeling of a prestressed concrete pipe pile-composite foundation", *KSCE J. Civil Eng.*, **19**(7), 2067-2074.
Yang, M., Su, H.Z. and Yan, X.Q. (2015b), "Computation and analysis of high rocky slope safety in a water conservancy project", *Discr. Dyn. Nat. Soc.*, 1-11.
Zhou, J.P., Yang, Z.Y. and Chen, G.F. (2006), "Status and challenges of high dam constructions in China", *J. Hydr. Eng.*, **37**(12), 1433-1438.

CC